Applied Physics Letters ARTICLE scitation.org/journal/apl

Infrared-active phonon modes and static dielectric constants in α-$(Al_xGa_{1-x})_2O_3$ ($0.18 \le x \le 0.54$) alloys

Cite as: Appl. Phys. Lett. **120**, 112202 (2022); doi: 10.1063/5.0085958
Submitted: 20 January 2022 · Accepted: 24 February 2022 ·
Published Online: 16 March 2022

Megan Stokey,[1,a)] Teresa Gramer,[1] Rafał Korlacki,[1] Sean Knight,[2] Steffen Richter,[2,3] Riena Jinno,[4,5] Yongjin Cho,[4] Huili Grace Xing,[4,6] Debdeep Jena,[4,6] Matthew Hilfiker,[1] Vanya Darakchieva,[2,3] and Mathias Schubert[1,2]

AFFILIATIONS

[1]Department of Electrical and Computer Engineering, University of Nebraska-Lincoln, Lincoln, Nebraska 68588, USA
[2]Terahertz Materials Analysis Center and Center for III-N Technology, C3NiT–Janzèn, Department of Physics, Chemistry and Biology (IFM), Linköping University, 58183 Linköping, Sweden
[3]NanoLund and Solid State Physics, Lund University, 22100 Lund, Sweden
[4]School of Electrical and Computer Engineering, Cornell University, Ithaca, New York 14853, USA
[5]Department of Electronic Science and Engineering, Kyoto University, Kyoto 615-8510, Japan
[6]Department of Material Science and Engineering, Cornell University, Ithaca, New York 14853, USA

Note: This paper is part of the APL Special Collection on Wide- and Ultrawide-Bandgap Electronic Semiconductor Devices.
[a)]**Author to whom correspondence should be addressed:** mstokey@huskers.unl.edu. **URL:** http://ellipsometry.unl.edu

ABSTRACT

We determine the composition dependence of the transverse and longitudinal optical infrared-active phonon modes in rhombohedral α-$(Al_xGa_{1-x})_2O_3$ alloys by far-infrared and infrared generalized spectroscopic ellipsometry. Single-crystalline high quality undoped thin-films grown on *m*-plane oriented α-Al_2O_3 substrates with $x = 0.18$, 0.37, and 0.54 were investigated. A single mode behavior is observed for all phonon modes, i.e., their frequencies shift gradually between the equivalent phonon modes of the isostructural binary parent compounds. We also provide physical model line shape functions for the anisotropic dielectric functions. We use the anisotropic high-frequency dielectric constants for polarizations parallel and perpendicular to the lattice *c* axis measured recently by Hilfiker *et al.* [Appl. Phys. Lett. **119**, 092103 (2021)], and we determine the anisotropic static dielectric constants using the Lyddane–Sachs–Teller relation. The static dielectric constants can be approximated by linear relationships between those of α-Ga_2O_3 and α-Al_2O_3. The optical phonon modes and static dielectric constants will become useful for device design and free charge carrier characterization using optical techniques.

Gallium oxides are a growing family of ultra-wide bandgap semiconductors with many established high-power applications.[1–4] While the thermodynamically stable *β*-phase Ga_2O_3 (bGO) is the most studied among the gallium oxide and related alloys materials family, the metastable α-phase of Ga_2O_3 (aGO) is now of emerging interest. One advantage of metastable aGO is the higher symmetry rhombohedral crystallographic structure and slightly higher bandgap than bGO.[5] It has been shown to grow reliably on *m*-plane sapphire,[6,7] and as such, there is great potential for heteroepitaxial technologies.[8–10] Similar to the ternary family of $Al_xGa_{1-x}N$, there is a large push to tune electronic and optical properties by alloying these films for device development. Alloys of α-$(Al,Ga)_2O_3$ cover a large range of bandgap energies far into the ultraviolet (UV-C) region ($E_g \approx 5.4$–8.8 eV) and represent a new class of ultra-wide bandgap semiconductors.[11,12] Recently, stable alloyed films have been successfully grown on corundum α-Al_2O_3.[13]

Reports on optoelectronic properties are not exhaustive. Bandgap energies and high-frequency dielectric constants were determined recently.[13–18] Hilfiker *et al.*[5] employed generalized spectroscopic ellipsometry and reported on the direction dependent bandgap energies and excitonic contributions, which differ for polarization parallel ($E_{g,\parallel} = 5.44$ eV) and perpendicular ($E_{g,\perp} = 5.46$ eV) to the lattice *c* axis in aGO. In another work, Hilfiker *et al.*[19] studied the same sample set discussed in this present Letter and reported on the high-frequency dielectric constants over the entire composition range for α-$(Al_xGa_{1-x})_2O_3$. Valence band offsets between amorphous SiO_2 and polycrystalline mixtures of α-$(Al_xGa_{1-x})_2O_3$ were estimated for laser

ablation deposited thin films by the "composition spread" method, and results indicate a possible valence band crossover for compositions around 50%; however, better sample quality and electric measurements may be required for confirmation.[20] In a recent work by Hilfiker *et al.*,[21] the anisotropic band-to-band transitions are determined for the same set of samples investigated here. A level crossover in the valence band order results in a change in lowest band-to-band transition polarization direction, where for α-Ga_2O_3, the lowest transition is polarized perpendicular to the lattice *c* axis and for α-Al_2O_3 the lowest transition is polarized parallel *c*.

Infrared and far-infrared spectra of semiconductor materials with polar lattice resonances can be used to determine optical phonon modes, and free charge carrier properties in the case of *n* or *p* type conductivity.[22] The optical phonons split into transverse optical (TO) and longitudinal optical (LO) phonon modes, where the latter are crucial for understanding of electrical and thermal transport properties, e.g., in electronic device designs. Knowledge of infrared-active phonon modes permits, for example, to determine free charge carrier properties using optical methods or to determine the state of strain of an epitaxial thin film.[22] Most recently, we reported a complete set of infrared-active phonon modes for aGO studying epitaxial thin films.[23] Therefore, we combined density functional theory analysis with generalized spectroscopic ellipsometry. Providing complete sets of all infrared and far-infrared active modes, a comprehensive view was possible in comparison between isostructural aGO and aAO. The irreducible sets of phonons are identical among the two compounds, while modifications occur between the phonon mode eigenvectors of equivalent modes among the two binaries. Such phonon mode eigenvector overlaps are of interest when studying the evolution of phonon modes into the alloys, where one element replaces gradually its isovalent group constituent. For aGO and aAO, four bands of phonon modes, each split into TO and LO modes, occur for polarization perpendicular to the lattice *c* direction, E_u, while two such bands occur for polarization parallel to *c* (A_{2u}).[23] When mixing two group-III oxide binary constituents within an isostructural lattice, aside from possible strain situations, the evolution of phonon modes commonly follows two scenarios: either the vibration bands merge and form a "single mode" behavior, i.e., a linear or otherwise continuous variation of TO and LO frequencies across the composition range, or a "two mode" behavior, where two bands extend over the composition range where each band vanishes into an impurity mode contribution within the infrared spectrum of its opposite binary compound. For example, for a "one mode" behavior, a TO mode of aGO will continuously change its frequency toward the TO mode of the equivalent phonon mode in aAO. In a two mode behavior, on the other hand, the aGO and aAO modes coexist as separate phonon modes at the same composition, throughout a certain composition range or the entire composition range. In our previous work, no data were available for phonon modes for alloy compositions. We hypothesized from the phonon mode eigenvector overlap (vector scalar product) calculations that all optical phonon modes could reveal a two mode behavior based on rather large changes within the lattice displacements of equivalent phonon modes in aGO and aAO. In this paper, we present the evolution of the infrared-active phonon modes and static dielectric constants determined from alloyed α-$(Al_xGa_{1-x})_2O_3$ films with an aluminum content of $x = 18\%$, 37%, and 54%. We employ the same line shape model approach discussed in our previous work for aGO epitaxial thin films and derive all phonon modes for the epitaxial alloy thin films. We find a one mode behavior for all phonon modes of the isostructural compounds. We discuss our findings in view of our previous results for aGO and aAO. Our results will become useful for future infrared spectral range analysis of phonon modes and free charge carrier properties in α-$(Al_xGa_{1-x})_2O_3$ thin film heterostructures. Our results will also become useful for future analysis of the influence of strain and stress onto the lattice mode properties in α-$(Al_xGa_{1-x})_2O_3$. We note that the samples investigated here are considered stress free according to previous investigations on similar samples.[13]

α-Ga_2O_3 crystallizes in the corundum structure ($R\bar{3}c$, space group 167), which is optically uniaxial and belongs to the trigonal crystal family. α-Al_2O_3 (sapphire) is isostructural to α-Ga_2O_3. Here, we observe from experiment and data analysis that alloying does not introduce additional modes and as such six total infrared-active modes are seen (two in the extraordinary A_u direction and four along the ordinary E_u direction). In this work, we identify all six TO-LO pairs for each alloying, which follow the TO-LO ordering rule as expected.[22,24]

A series of three α-$(Al_xGa_{1-x})_2O_3$ samples were investigated here with compositions of $x = 0.18$, 0.37, and 0.54. All samples were heteroepitaxially grown as (10 $\bar{1}$ 0) oriented thin films on *m*-plane oriented α-Al_2O_3 substrates via plasma-enhanced molecular beam epitaxy (PAMBE).[13] The substrates were treated with an oxygen plasma for ten minutes at $T = 800\,^\circ$ C before growth and then were maintained at 650° 650 °C during growth. A radio frequency plasma source was used with an oxygen flow rate of 0.5 sccm to create active oxygen species. The chamber pressure was kept at 10^{-5} Torr during the deposition. X-ray reflectivity measurements were done after the growth to determine the epitaxial layers' thicknesses $d = 56.7$, 66, and 84.3 nm for $x = 0.18$, 0.37, and 0.54, respectively. Atomic force microscopy indicated a root mean square roughness of 0.95, 0.78, and 0.97 nm, respectively. By using asymmetrical reciprocal space map analysis, the α-$(Al_xGa_{1-x})_2O_3$ films were determined to follow the *m*-plane orientation of the substrate. The epitaxial thin films were found unstrained. Further information regarding growth and characterization can be found in Jinno *et al.*[13]

Generalized spectroscopic ellipsometry is an optical measurement technique that can determine the anisotropic optical properties of a material. At each wavenumber, the Mueller matrix of the material is determined. The Mueller matrix relates the Stokes vector components before and after interaction with a sample as follows:

$$\begin{pmatrix} S_0 \\ S_1 \\ S_2 \\ S_3 \end{pmatrix}_{\text{output}} = \begin{pmatrix} M_{11} & M_{12} & M_{13} & M_{14} \\ M_{21} & M_{22} & M_{23} & M_{24} \\ M_{31} & M_{32} & M_{33} & M_{34} \\ M_{41} & M_{42} & M_{43} & M_{44} \end{pmatrix} \begin{pmatrix} S_0 \\ S_1 \\ S_2 \\ S_3 \end{pmatrix}_{\text{input}}, \quad (1)$$

with Stokes vector components defined here by $S_0 = I_p + I_s$, $S_1 = I_p - I_s$, $S_2 = I_{45} - I_{-45}$, $S_3 = I_{\sigma+} - I_{\sigma-}$. Here, I_p, I_s, I_{45}, I_{-45}, $I_{\sigma+}$, and $I_{\sigma-}$ denote the intensities for the *p*-, *s*-, +45°, and −45°, right handed, and left handed circularly polarized light components, respectively.[22]

Two different instruments were used to take generalized spectroscopic ellipsometry measurements in ambient conditions. Our infrared data (450–1200 cm^{-1}) were measured on a commercially available variable angle of incidence spectroscopic ellipsometer (VASE) (IR-VASE

Mark-II; J. A. Woollam Co., Inc.). The far-infrared data (100–450 cm^{-1}) were measured on an in-house built FIR-VASE system.[25,26] To capture the anisotropic nature of these samples, two angles of incidence were selected as $\Phi_a = 50°$ and 70°, and data at four azimuthal rotations (0°, 45°, 90°, and 135°) were measured. This set of data permitted to fully observe and account for the uniaxial optical properties of the samples where the two materials involved, sapphire and the α-$(Al_xGa_{1-x})_2O_3$ thin films, have a common orientation of their optical axes parallel to the surface. Note that only the IR ellipsometer instrument is capable of measuring the fourth row elements (excluding M_{44}) of the Mueller matrix, and as a result, these are only available above approximately 250 cm^{-1}.

Analysis of these data was completed using WVASE32™ (J. A. Woollam Co., Inc.). The model for each sample is structurally similar to the uniaxial model as described in Stokey *et al.*[23] with the Euler angles adjusted and thickness changed accordingly. Similar to Ref. 23, we render the dielectric functions for both substrate and thin film using the four-parameter semi-quantum (FPSQ) model, described by Gervais and Periou,[27]

$$\varepsilon_j = \varepsilon_{\infty,j} \prod_{l=1}^{N} \frac{\omega_{\mathrm{LO},l,j}^2 - \omega^2 - i\omega\gamma_{\mathrm{LO},l,j}}{\omega_{\mathrm{TO},l,j}^2 - \omega^2 - i\omega\gamma_{\mathrm{TO},l,j}}, \tag{2}$$

wherein one defines the TO and LO mode frequency and broadening parameters ($\omega_{\mathrm{TO},l,j}$, $\gamma_{\mathrm{TO},l,j}$, $\omega_{\mathrm{LO},l,j}$, $\gamma_{\mathrm{LO},l,j}$), and where $\varepsilon_{\infty,j}$ is the high-frequency dielectric constant. Here, j denotes the polarization direction ($j = \parallel$ for polarization parallel to the lattice c direction—A_{2u} modes, or $j = \perp$ to c—E_u modes) and N denotes the number of phonon mode pairs in either direction. For sapphire, we use previous results for all parameters.[28] For the α-$(Al_xGa_{1-x})_2O_3$ thin films, we include $N = 4$ sets for $j = \perp$, and $N = 2$ sets for $j = \parallel$. For model calculations of our data, we use $\varepsilon_{\infty,j}$ values reported previously by Hilfiker *et al.*[19] With the Lydanne–Sachs–Teller (LST) relationship, we then obtain[29]

$$\frac{\varepsilon_{\mathrm{DC},j}}{\varepsilon_{\infty,j}} = \prod_{l=1}^{N} \frac{\omega_{\mathrm{LO},l,j}^2}{\omega_{\mathrm{TO},l,j}^2}, \tag{3}$$

which permits us to replace the high-frequency constants with the static dielectric constants $\varepsilon_{\mathrm{DC},j}$ for both polarizations, and which then become adjustable parameters in our best model calculations.

The best-match model calculations over experimental Mueller matrix data are available for each sample in the supplementary material. An excellent match is obtained between our best-match model calculated data and experimental data, for each sample. All samples behave optically similar, except for subtle variations due to variations in the phonon mode parameters.

In our best-match model analysis for the α-$(Al_xGa_{1-x})_2O_3$ thin films, we identified as many phonon mode pairs for both polarization directions as we recorded previously for α-Ga_2O_3 and sapphire. Hence, we conclude that all modes in this alloy system, at least within the composition range covered in this work, reveal a one mode behavior. Figures 1 and 2 depict the resultant infrared model line shapes in terms of the imaginary parts of the dielectric function and its inverse dielectric function. These two spectra sets peak at the TO and LO mode frequencies, respectively, and therefore, provide the most obvious access to the underlying phonon mode properties. Included into the figures are the respective functions obtained previously for

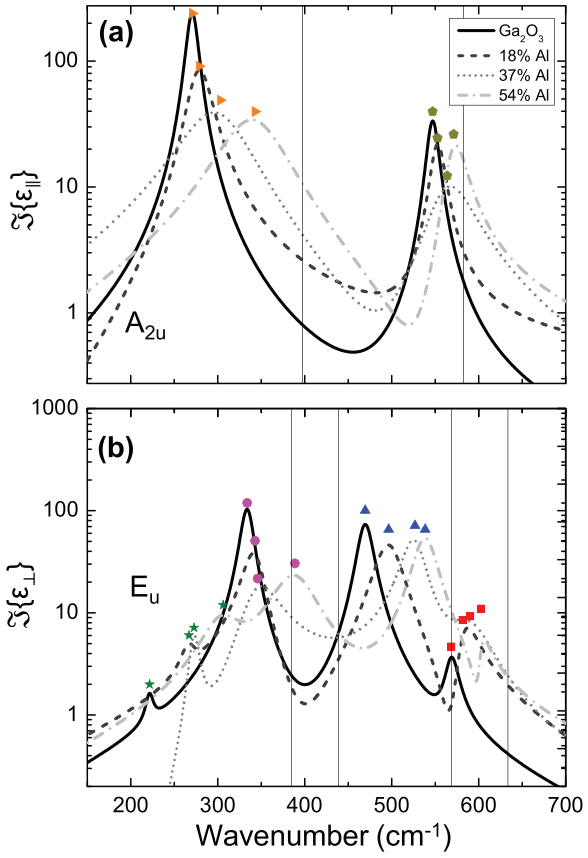

FIG. 1. The imaginary part of the dielectric functions for all samples investigated here. (a) $\Im\{\varepsilon_\parallel\}$ and (b) $\Im\{\varepsilon_\perp\}$. Data for α-Ga_2O_3 are included for comparison. Vertical lines indicate TO frequencies for α-Al_2O_3. Symbols indicate peak positions and thereby TO modes of the ternary alloys.

α-Ga_2O_3, for comparison, and also include identification for the phonon mode frequencies of sapphire. One can observe a general increase in broadening of the phonon features as well as a general increase in frequency with the increase in Al composition.

From these best match model calculations, we extract the TO and LO mode frequency parameters of each mode pair and for each alloying and plot them along with linear trend lines in Figs. 3 and 4. These trendlines are calculated as a linear evolution from the experimentally found mode frequencies for the binary parent compounds, α-Ga_2O_3[23] and α-Al_2O_3.[28] The best-match mode calculated frequency parameters are listed in Table I, while the respective broadening parameters are listed in Table II. As seen in Figs. 3 and 4, all phonon modes evolve in near linear fashion upward in frequency with the increasing Al composition. This upward shift in frequency can be predicted by the replacement of heavy Ga atoms with lighter Al atoms. We observe some deviation from the linear trendlines in the $x = 37\%$ sample, and while some residual strain effect cannot be ruled out, it was previously obtained that the samples studied are mostly unstrained.[13]

Figure 5 depicts the static dielectric constants obtained for our samples here. Included are also data for α-Ga_2O_3 to α-Al_2O_3. Data

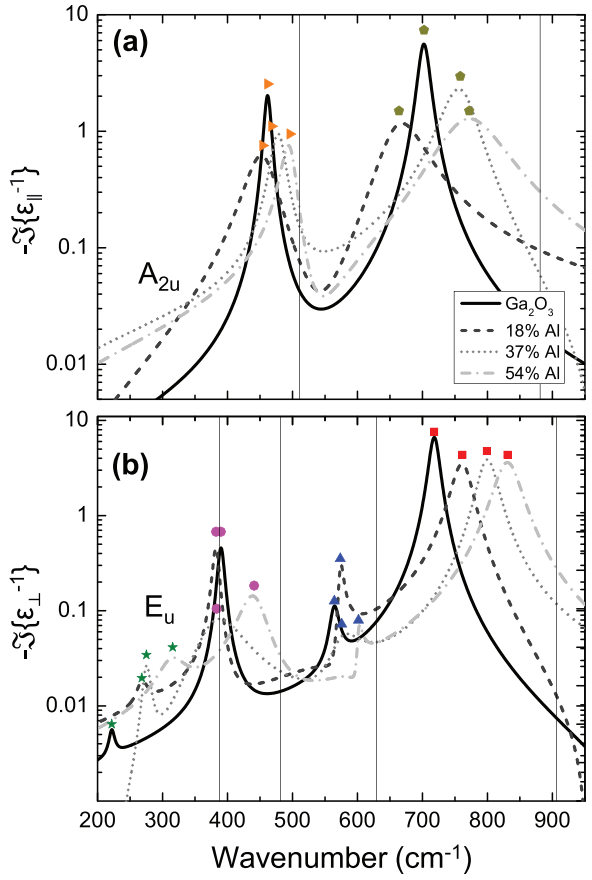

FIG. 2. The negative imaginary part of the inverse dielectric functions for all samples investigated here. (a) $\Im\{-\varepsilon_{\parallel}^{-1}\}$ and (b) $\Im\{-\varepsilon_{\perp}^{-1}\}$. Data for α-Ga_2O_3 are included for comparison. Vertical lines indicate LO frequencies for α-Al_2O_3. Symbols indicate peak positions and, thereby, LO modes of the ternary alloys.

were calculated via the LST-relationship using the TO and LO modes obtained here and values for the high-frequency constants reported by Hilfiker *et al.* All parameters are also listed in Table III. Largely, all values follow a linear trend between the binary parent compounds. We note that these values are of high interest for design rationale of electronic device structures. As can be seen, the differences between the ordinary and extraordinary dielectric constants decrease with the increasing Al composition, while also both values decrease between α-Ga_2O_3 and α-Al_2O_3. The latter is reasonable since Ga is larger than Al and causes overall a larger total electronic polarizability.[30] We note here that the static dielectric constant is a measure of the entire spectral linear polarizability representing all polar and electronic contributions including x-ray core electron excitations.

In Table IV, we further show the calculated index of refraction and birefringence values for quasi-static (n_{DC}) and below-bandgap (n_{∞}) values. The latter are obtained from Hilfiker *et al.*[20] and are the value of the index of refraction at the wavelength within the bandgap at which the change in index with wavelength vanishes. The quasi-static values and birefringence are shown in Fig. 6. The anisotropy (Table III) and birefringence are quite large. All values reduce with the

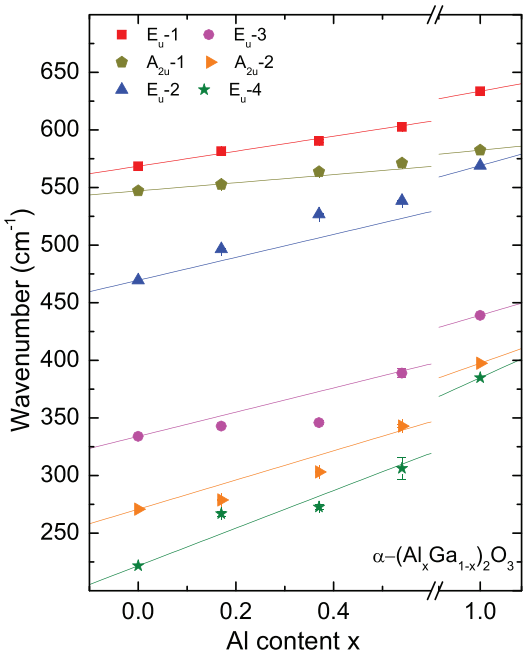

FIG. 3. Best match model calculated phonon mode parameters (TO; symbols) for all observed phonon modes for the α-$(Al_xGa_{1-x})_2O_3$ thin films. Lines are linear interpolations between corresponding phonon modes of the binary compounds. Error bars are included on each data point, though many are too small to be seen behind the symbol.

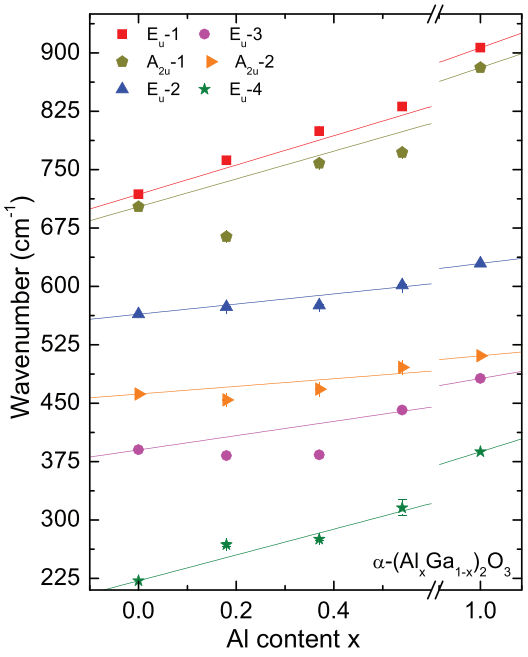

FIG. 4. Same as Fig. 3 but for LO modes. Lines are linear interpolations between corresponding phonon modes of the binary compounds.

TABLE I. Best-match model parameters for α-$(Al_xGa_{1-x})_2O_3$ TO and LO phonon modes. The last digit, which is determined within the 90% confidence interval, is indicated with brackets.

Mode	ω_{TO} x = 0 Ref. 23	ω_{TO} x = 0.18 This work	ω_{TO} x = 0.37 This work	ω_{TO} x = 0.54 This work	ω_{TO} x = 1 Ref. 28	ω_{LO} x = 0 Ref. 23	ω_{LO} x = 0.18 this work	ω_{LO} x = 0.37 This work	ω_{LO} x = 0.54 This work	ω_{LO} x = 1 Ref. 28
A_{2u}-1	547.1	552.(6)	563.(7)	571.(3)	582.41	702.3	663.(9)	758.(3)	771.(9)	881.1
A_{2u}-2	292.81	278.(8)	26(9)	270.(6)	453.43	461.8	454.(3)	467.(9)	496.(1)	510.9
E_u-1	568.5	581.(6)	590.(3)	602.(5)	633.6	718.3	761.(8)	799.(4)	831.(0)	906.6
E_u-2	469.5	496.(5)	526.(7)	538.4(4)	569.0	564.3	573.(5)	575.(8)	601.(6)	629.5
E_u-3	334.0	342.(9)	345.(9)	388.(9)	439.0	390.0	382.(5)	383.(5)	441.(1)	481.7
E_u-4	221.7	266.(9)	272.(7)	306.(2)	384.9	221.9	268.(2)	275.(2)	315.(6)	387.6

TABLE II. Same as Table I for broadening parameters. Values marked with an asterisk were kept fixed during analysis.

Mode	γ_{TO} x = 0.18	γ_{TO} x = 0.37	γ_{TO} x = 0.54	γ_{LO} x = 0.18	γ_{LO} x = 0.37	γ_{LO} x = 0.54
A_{2u}-1	8.(2)	17.(7)	27.(0)	50*	50*	70*
A_{2u}-2	41.(4)	50*	70*	60*	45.(5)	18.(5)
E_u-1	9.(5)	47.(1)	12.(4)	37.(2)	45.(3)	42.(5)
E_u-2	33.(9)	39.(1)	25.(7)	13.(5)	68.(2)	5.(8)
E_u-3	37.(8)	38.(3)	67.(4)	32.(8)	50*	59.(6)
E_u-4	60*	26.(5)	50*	47.(9)	50*	50*

increasing aluminum content. The quasi-static birefringence is positive throughout. The below-bandgap anisotropy and birefringence, on the other hand, are negative (Table IV), and much smaller than their corresponding values at quasi-static frequencies.

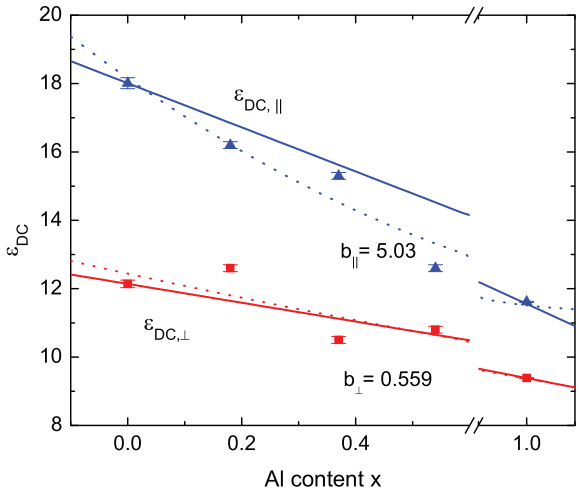

FIG. 5. Static dielectric constants as listed in Table III shown against their linear trendlines (solid) between corresponding values for α-Ga_2O_3 and α-Al_2O_3. Blue triangles denote the ordinary axis values, and red squares denote the extraordinary axis values. Dotted lines show quadratic fits with bowing parameters $b_{||} = 5.03$ and $b_{\perp} = 0.559$.

TABLE III. Static dielectric constants calculated using the LST-relationship for α-$(Al_xGa_{1-x})_2O_3$ alloys. High-frequency dielectric constants were held constant during our analysis at the values reported by Hilfiker *et al.* Anisotropy values $\Delta\varepsilon = \varepsilon_{||} - \varepsilon_{\perp}$ for both high-frequency and static dielectric constants are provided.

x =	$\varepsilon_{DC,\|\|}$	$\varepsilon_{DC,\perp}$	$\Delta\varepsilon_{DC}$	$\varepsilon_{\infty,\|\|}$	$\varepsilon_{\infty,\perp}$	$\Delta\varepsilon_{\infty}$
0.00	18.0(1)[a]	12.1(4)[a]	5.87	3.7(6)[b]	3.8(6)[b]	−0.1
0.18	16.(2)	12.(6)	3.6	3.60(4)[c]	3.68(8)[c]	−0.084
0.37	15.(3)	10.(5)	4.8	3.41(6)[c]	3.47(9)[c]	−0.063
0.54	12.(6)	10.(8)	1.8	3.29(4)[c]	3.33(1)[c]	−0.037
1.00	11.61(4)[d]	9.38(5)[d]	2.229	3.07(2)[d]	3.07(7)[d]	−0.005

[a]Reference 23.
[b]Reference 5.
[c]Reference 19.
[d]Reference 28.

In our previous work on α-Ga_2O_3 thin films, we provide calculated eigenvector overlap values for each Brillouin zone center phonon mode between α-Ga_2O_3 and α-Al_2O_3.[23] While these did reveal some interesting similarities between different modes in each material, the overall trend was that the corresponding modes (e.g., E_u-2 in each material) had the highest overlap values. Hence, a gradual mode frequency shift across the alloy system could have also been predicted, which is now seen with this set of experiments discussed in the present work.

In conclusion, we have determined the TO and LO mode frequency and broadening parameter dependencies on the Al composition in

TABLE IV. Index of refraction calculated from Table III values (including values taken from Refs. 5, 19, 23, and 28) for α-$(Al_xGa_{1-x})_2O_3$ alloys. Birefringence values $\Delta n = \sqrt{\varepsilon_{||}} - \sqrt{\varepsilon_{\perp}}$ for both below-bandgap and quasi-static values are also provided.

x =	$n_{DC,\|\|}$	$n_{DC,\perp}$	Δn_{DC}	$n_{\infty,\|\|}$	$n_{\infty,\perp}$	Δn_{∞}
0.00	4.24	3.48	0.76	1.94	1.96	−0.026
0.18	4.02	3.55	0.480	1.897	1.920	−0.0231
0.37	3.91	3.24	0.671	1.848	1.865	−0.0169
0.54	3.55	3.29	0.263	1.814	1.825	−0.0102
1.00	3.408	3.063	0.344	1.753	1.754	−0.0014

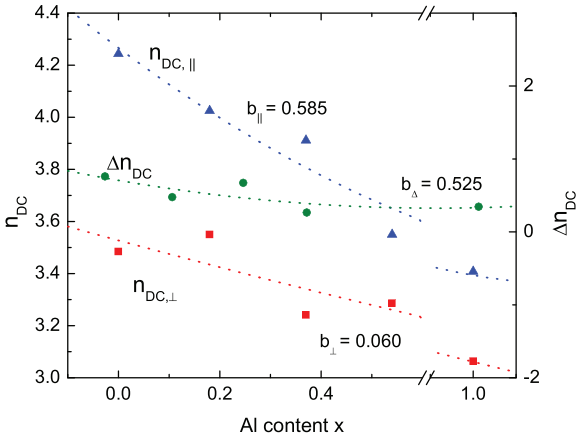

FIG. 6. Static index of refraction values as listed in Table IV. Blue triangles denote the ordinary axis values, red squares denote the extraordinary axis values, and green circles denote the birefringence values. Dotted lines show quadratic fits with bowing parameters $b_{\|} = 0.585$, $b_{\perp} = 0.060$, and $b_{\Delta} = 0.0525$.

rhombohedral α-$(Al_xGa_{1-x})_2O_3$. All phonon modes reflect a single mode behavior. All observed frequencies shift gradually and approximately linearly between the equivalent phonon modes of the isostructural binary parent compounds. We also determined the dielectric constants for electric field polarizations parallel and perpendicular to the lattice *c* direction, which will become useful for rationale device design. We provide all model line shape function parameters for the epitaxial thin films investigated here, which will become useful for future analysis of device heterostructure samples, for example, to determine free charge carrier contributions using infrared optical techniques. Phonon mode and static dielectric constant properties, including their anisotropy, will become very useful for future thermal and electronic transport characterization and device design, for example.

See the supplementary material file for experimental and best-match model Mueller matrix figures for all samples in this study as well as Born effective charge information.

This work was supported in part by the National Science Foundation (NSF) under Award Nos. NSF DMR 1808715 and NSF/EPSCoR RII Track-1: Emergent Quantum Materials and Technologies (EQUATE), Award No. OIA-2044049; and by Air Force Office of Scientific Research under Award Nos. FA9550-18-1-0360, FA9550-19-S-0003, and FA9550-21-1-0259; and by ACCESS, an AFOSR Center of Excellence, under Award No. FA9550-18-1-0529, and by the Knut and Alice Wallenbergs Foundation award "Wide-bandgap semiconductors for next generation quantum components." M.S. acknowledges the University of Nebraska Foundation and the J. A. Woollam Foundation for support. R.J. acknowledges the support from JSPS Overseas Challenge Program for Young Researchers No. 1080033. This work was also supported in part by the Swedish Research Council VR Award No. 2016-00889, the Swedish Energy Agency under Award No. P453396-1, the Swedish Foundation for Strategic Research Grant Nos. RIF14-055 and EM16-0024, by the Swedish Governmental Agency for Innovation Systems VINNOVA under the Competence Center Program Grant No. 2016-05190, and by the Swedish Government Strategic Research Area in Materials Science on Functional Materials at Linköping University, Faculty Grant SFO Mat LiU No. 2009-00971.

AUTHOR DECLARATIONS

Conflict of Interest

The authors have no conflicts of interest to disclose.

DATA AVAILABILITY

The data that support the findings of this study are available from the corresponding author upon reasonable request.

REFERENCES

[1]M. Higashiwaki, K. Sasaki, A. Kuramata, T. Masui, and S. Yamakoshi, Phys. Status Solidi A **211**, 2126 (2014).
[2]M. Higashiwaki and G. H. Jessen, Appl. Phys. Lett. **112**, 060401 (2018).
[3]Z. Xia, H. Chandrasekar, W. Moore, C. Wang, A. J. Lee, J. McGlone, N. K. Kalarickal, A. Arehart, S. Ringel, F. Yang, and S. Rajan, Appl. Phys. Lett. **115**, 252104 (2019).
[4]J. Zhang, J. Shi, D.-C. Qi, L. Chen, and K. H. L. Zhang, APL Mater. **8**, 020906 (2020).
[5]M. Hilfiker, R. Korlacki, R. Jinno, Y. Cho, H. G. Xing, D. Jena, U. Kilic, M. Stokey, and M. Schubert, Appl. Phys. Lett. **118**, 062103 (2021).
[6]M. Bosi, P. Mazzolini, L. Seravalli, and R. Fornari, J. Mater. Chem. C **8**, 10975 (2020).
[7]M. J. Tadjer, Electrochem. Soc. Int. **27**, 49 (2018).
[8]Z. A. Jian, Y. Oshima, S. Wright, K. Owen, and E. Ahmadi, Semic. Sci. Technol. **34**, 035006 (2019).
[9]M. Oda, R. Tokuda, H. Kambara, T. Tanikawa, T. Sasaki, and T. Hitora, Appl. Phys. Express **9**, 021101 (2016).
[10]G. Dang, T. Kawaharamura, M. Furuta, and M. Allen, IEEE Trans. Electron Devices **62**, 3640 (2015).
[11]J. Varley, J. Mater. Res. **36**, 4790 (2021).
[12]J. A. Spencer, A. L. Mock, A. G. Jacobs, M. Schubert, Y. Zhang, and M. J. Tadjer, Appl. Phys. Rev. **9**, 011315 (2022).
[13]R. Jinno, C. S. Chang, T. Onuma, Y. Cho, S.-T. Ho, D. Rowe, M. C. Cao, K. Lee, V. Protasenko, D. G. Schlom, D. A. Muller, H. G. Xing, and D. Jena, Sci. Adv. **7**, eabd5891 (2021).
[14]H. Ito, K. Kaneko, and S. Fujita, Jpn. J. Appl. Phys., Part 1 **51**, 09LD16 (2012).
[15]G. T. Dang, T. Yasuoka, Y. Tagashira, T. Tadokoro, W. Theiss, and T. Kawaharamura, Appl. Phys. Lett. **113**, 062102 (2018).
[16]Z. Chen, M. Arita, K. Saito, T. Tanaka, and Q. Guo, AIP Adv. **11**, 035319 (2021).
[17]T. Uchida, R. Jinno, S. Takemoto, K. Kaneko, and S. Fujita, Jpn. J. Appl. Phys., Part 1 **57**, 040314 (2018).
[18]M. Kracht, A. Karg, M. Feneberg, J. Bläsing, J. Schörmann, R. Goldhahn, and M. Eickhoff, Phys. Rev. Appl. **10**, 024047 (2018).
[19]M. Hilfiker, U. Kilic, M. Stokey, R. Jinno, Y. Cho, H. G. Xing, D. Jena, R. Korlacki, and M. Schubert, Appl. Phys. Lett. **119**, 092103 (2021).
[20]X. Xia, C. Fares, F. Ren, A. Hassa, H. von Wenckstern, M. Grundmann, and S. J. Pearton, ECS J. Solid State Sci. Technol. **10**, 113007 (2021).
[21]M. Hilfiker, U. Kilic, M. Stokey, R. Jinno, H. G. Xing, D. Jena, R. Korlacki, and M. Schubert, "Anisotropic dielectric function, direction dependent bandgap energy, band order, and indirect to direct gap cross over in α-$(Al_xGa_{1-x})_2O_3$ $(0 \leq x \leq 1)$," Appl. Phys. Lett. (submitted) (2022).
[22]M. Schubert, *Infrared Ellipsometry on Semiconductor Layer Structures: Phonons, Plasmons and Polaritons*, Springer Tracts in Modern Physics Vol. 209 (Springer, Berlin, 2004).
[23]M. Stokey, R. Korlacki, M. Hilfiker, S. Knight, S. Richter, V. Darakchieva, R. Jinno, Y. Cho, H. G. Xing, D. Jena, Y. Oshima, K. Khan, E. Ahmadi, and M. Schubert, Phys. Rev. Mater. **6**, 014601 (2022).

[24]G. Venkataraman, L. A. Feldkamp, and V. C. Sahni, *Dynamics of Perfect Crystals* (The MIT Press, Cambridge, Massachusetts/London, England, 1975).
[25]P. Kühne, C. M. Herzinger, M. Schubert, J. A. Woollam, and T. Hofmann, Rev. Sci. Instrum. **85**, 071301 (2014).
[26]P. Kühne, N. Armakavicius, V. Stanishev, C. M. Herzinger, M. Schubert, and V. Darakchieva, IEEE Trans. Terahertz Sci. Technol. **8**, 257 (2018).
[27]F. Gervais and B. Piriou, J. Phys. C **7**, 2374 (1974).
[28]M. Schubert, T. E. Tiwald, and C. M. Herzinger, Phys. Rev. B **61**, 8187 (2000).
[29]R. H. Lyddane, R. Sachs, and E. Teller, Phys. Rev. **59**, 673 (1941).
[30]R. H. Petrucci, *General Chemistry: Principles and Modern Applications*, 11th ed. (Pearson, Toronto, 2017).